THE ASTROPHYSICAL JOURNAL, 470:790–796, 1996 October 20

DETECTION OF DYNAMICAL STRUCTURES USING COLOR GRADIENTS IN GALAXIES

A. C. QUILLEN,[1] SOLANGE V. RAMÍREZ,[2] AND JAY A. FROGEL[3]
Astronomy Department, Ohio State University, 174 West 18th Avenue, Columbus, OH 43210
Received 1995 September 22; accepted 1996 May 21

ABSTRACT

We describe a technique that uses radial color gradients in disk galaxies to detect the presence of bulk noncircular motion or elliptical orbits. In a disk galaxy with both a radial color gradient and noncircular motion, isochromes, or isocolor contours, should follow the shape of closed stellar orbits, and the ellipticity of the isophotes should vary as a function of wavelength. A difference in the ellipticity of isochromes and the isophotes can be used to detect the presence of noncircular motion. A model galaxy is constructed which demonstrates this phenomenon. The difference between isochrome and isophote ellipticity is directly related to the ellipticity of the potential. This provides a new way to measure the ellipticity of the dark matter in the outer parts of galaxies.

As an example, we apply this technique to two dwarf galaxies, NGC 1800 and NGC 7764. We detect a bar in NGC 1800 which has only previously been suggested from the H I velocity field. In NGC 7764 there is no color gradient along its bar, so we cannot detect noncircular motion in this region; however, ellipticities observed in a star-forming ring at the end of the bar are consistent with this ring being located near the corotation resonance.

Subject headings: galaxies: individual (NGC 1800, NGC 7764) — galaxies: kinematics and dynamics — galaxies: photometry — galaxies: spiral

1. INTRODUCTION

Previous studies of observational signatures of noncircular or elliptical motion in galaxies include Franx, van Gorkom, & de Zeeuw (1994), Sackett et al. (1994), Franx & de Zeeuw (1992), Staveley-Smith et al. (1990), and de Zeeuw & Franx (1989). These studies explore how twists in the velocity field coupled with measurements of the ellipticities of the isophotes (in one wavelength band) in a galaxy can be used to constrain the ellipticity of the halo or the axis ratios of a triaxial gravitational potential. Many of these studies have noted (e.g., de Zeeuw & Franx 1989; Franx et al. 1994) that there should be a difference between isophote ellipticity and orbit ellipticity; however, this difference has not been exploited by using the information available in color maps.

Multiband imaging studies of late-type galaxies have found that these galaxies almost always have radial color gradients (e.g., de Jong 1994). Color maps often reveal underlying structures such as bars and rings (e.g., Buta 1990). Although color gradients have been used to study the dynamics of different stellar populations in elliptical galaxies (e.g., Thomsen & Baum 1989), little has been done using color gradients to derive dynamical information in spiral galaxies. In this paper we show how the ellipticity of the isophotes should vary as a function of wavelength in a disk galaxy that has both a radial color gradient and noncircular stellar motion. This effect, once detected, can be used to detect and study bars and other nonaxisymmetric structures, such as a triaxial halo. We illustrate with a model galaxy that has a color gradient such that when the potential is nonaxisymmetric the isophotes have different shapes than the isochromes. We show how the ellipticity of the potential can be derived from the orbit and isophote ellipticities.

To illustrate a preliminary use of this phenomenon, we search for it in two dwarf galaxies, NGC 1800 and NGC 7764. Dwarf galaxies are a promising place to search for this effect because they commonly harbor bars and other asymmetric structures. Their low dust content facilitates measuring the ellipticity of the isophotes, and they commonly have color gradients (e.g., Quillen, Ramírez, & Frogel 1995). Our data are a preliminary part of a survey of 200–300 galaxies that will produce a library of photometrically calibrated images of late-type galaxies from 0.4 to 2.2 μm.

2. COLOR GRADIENTS AND NONCIRCULAR MOTION

In disk galaxies the velocity dispersion of the stars is typically far smaller than the rotational velocity, so that many stars are in nearly circular orbits in a plane. In the epicyclic approximation stars can be considered to be oscillating at the epicyclic frequency about circular orbits. If the galaxy is perturbed by an elliptical potential, then the closed orbits are elliptical instead of circular. The stars are then considered to be oscillating about a family of closed elliptical orbits. When the stellar velocity dispersion is small, as is commonly the case in late-type galaxies, the appearance of the galaxy is determined by the structure of these closed orbits.

Consider a galaxy with a stationary bar-shaped perturbation to the potential. Closed orbits in this galaxy have an elliptical shape. Usually the velocity of a star in a closed elliptical orbit is slowest at the apocenter or major-axis vertex of the ellipse. This causes the galaxy mass surface density or surface brightness along this orbit to increase at the apocenter. The isophotes of the galaxy are therefore determined by the radial light distribution and the shapes and velocity variation in the orbits. The mass continuity equation for a steady state system can be used to predict the surface density of the galaxy from the azimuthally averaged stellar surface density and the structure of the closed orbits.

[1] quillen@payne.mps.ohio-state.edu.
[2] Visiting Astronomer, Cerro Tololo Inter-American Observatory. CTIO is operated by AURA, Inc., under contract to the National Science Foundation.
[3] Visiting Associate of the Observatories, Carnegie Institution of Washington.

In other words, by considering the volume of a small parcel, the density variation about the orbit can be determined from the velocity and volume change of the parcel. The difference between isophote and orbit ellipticities has been noted previously (e.g., de Zeeuw & Franx 1989; Franx et al. 1994).

Most galaxies exhibit radial color gradients from variations in stellar population and dust distribution. This means that the azimuthally averaged surface intensity is a function of wavelength. Differential rotation causes the stellar population to be evenly distributed about the closed orbits, so that these orbits are isopopulation contours. These contours should also be isochromes in a color map. Because the closed orbits in an axisymmetric galaxy are circular, the isophotes and isochromes are coincident and also circular. However, in a nonaxisymmetric galaxy the isophote shapes depend on orbit structure as well as the azimuthally averaged surface intensity. This implies that the isophote shapes vary as a function of wavelength when there is both noncircular motion and a color gradient. The ellipticities of the isochromes should differ from the ellipticities of the isophotes. Observation of this behavior can be used to detect and study the presence of noncircular motion.

2.1. *The Case of Small Ellipticity*

Orbits that are approximately elliptical with a small ellipticity can be described by a radius

$$R(r_0, \theta) = r_0\left[1 + \frac{\epsilon_r(r_0)}{2}\cos 2\theta\right], \tag{1}$$

where ϵ_r is the ellipticity of the orbit. On an individual orbit with coordinates given by the previous equation, we can define a speed and a surface density

$$v(R(r_0, \theta)) = v_0(r_0)\left[1 + \frac{\epsilon_v(r_0)}{2}\cos 2\theta\right], \tag{2}$$

$$\Sigma(R(r_0, \theta)) = \Sigma_0(r_0)\left[1 + \frac{\epsilon_\Sigma(r_0)}{2}\cos 2\theta\right]. \tag{3}$$

The ellipticity of the isophotes, ϵ_D, is determined by the semimajor and semiminor axes $r_{\max}$ and $r_{\min}$, which have equivalent surface densities, and can be estimated by $\epsilon_D = (r_{\max} - r_{\min})/r_{\min}$. Since the density is related to the velocity using the mass continuity equation, Σ^{-1} is proportional to the velocity times the area element $dA/dr\,d\theta$ in a segment of a thin shell along each orbit. For the shape of the orbits given above, the area element is

$$\frac{dA(R(r_0, \theta))}{dr\,d\theta} = r_0\left[1 + (\epsilon_r + r_0\epsilon_r')\frac{\cos 2\theta}{2}\right], \tag{4}$$

where $\epsilon_r' = d\epsilon_r/dr$. On the orbit the density varies with ellipticity,

$$\epsilon_\Sigma = -\epsilon_r - \epsilon_v - r_0\epsilon_r'. \tag{5}$$

The ellipticity of the isophotes is then

$$\epsilon_D = \epsilon_r - \frac{\epsilon_\Sigma\Sigma_0}{\Sigma_0' r}, \tag{6}$$

where $\Sigma_0' = d\Sigma_0/dr$. For an exponential disk with density $\Sigma(r) \propto \exp(-r/r_D)$ and scale length r_D,

$$\epsilon_D = \epsilon_r - \frac{r_D}{r}(\epsilon_r + \epsilon_v + r\epsilon_r'). \tag{7}$$

For example, a logarithmic potential $\Phi = v_c^2 \ln s$, where $s = (x^2/q^2 + y^2)^{1/2}$ and $\epsilon = 1 - q$, has orbits with $\epsilon_r = \epsilon$, $\epsilon_v = -2\epsilon$, and $\epsilon_\Sigma = \epsilon$, and isophotes with ellipticity $\epsilon_D = \epsilon(1 + r_D/r)$ (as has been previously noted in Franx et al. 1994) for an exponential disk with scale length r_D.

Since the isophote ellipticity ϵ_D depends on $\Sigma_0(r)$, it also depends upon the band in which the galaxy is observed when there is a color gradient. Differences between isophotes and color contours can be used to detect the presence of noncircular motion. The difference in ellipticity is a maximum and therefore easiest to measure where $\Sigma_0'(r)$ is small and the surface brightness gradient is shallow.

Two angles are required to describe the orientation of a galaxy: an inclination or tilt angle, and the position angle of the tilt with respect to the major axis of the gravitational potential. A projected ellipse appears to have a different position angle and ellipticity than its true position angle and ellipticity. If the ellipticities and position angles of the isophotes are known at more than two radii and vary as a function of radius, then the projection angles of the galaxy can be uniquely determined (see eqs. [3.12]–[3.14] in de Zeeuw & Franx 1989).

2.1.1. *Probing the Ellipticity of the Gravitational Potential*

Once the orientation of the galaxy is known, it is possible to probe directly the shape of the gravitational potential in the plane of the galaxy from the true orbit and isophote ellipticities. In the epicyclic approximation for a gravitational potential, $\Phi(r, \theta) = \Phi_0(r) + \Phi_1(r)\cos 2\theta$, with $\Phi_1/\Phi_0 \ll 1$, the size of the nonaxisymmetric perturbation is (Binney & Tremaine 1987)

$$\Phi_1 = -\frac{v_c(r)^2}{2}(\epsilon_r + \epsilon_v)\left(1 - \frac{\Omega_p}{\Omega}\right), \tag{8}$$

where ϵ_v can be determined from the isophotes and isochromes using equations (5) and (6). Here v_c is the circular velocity given by $d\Phi_0/dr = v_c^2/r$, and $\Omega = v_c/r$ is the angular rotation rate. If the potential is rotating, Ω_p is the pattern speed of the nonaxisymmetric component of the potential. When the potential is fixed, $\Omega_p = 0$. We define the ellipticity of the potential in the same way as we define the isophote ellipticity and find that it is $\epsilon_\Phi = -2\Phi_1/v_c^2$. Thus equation (8) above simplifies to

$$\epsilon_\Phi = (\epsilon_r + \epsilon_v)\left(1 - \frac{\Omega_p}{\Omega}\right), \tag{9}$$

and we see that the orbit and isophote ellipticities can be used directly to probe the ellipticity of the potential.

The most common situation in which the potential rotates is in a barred galaxy. Over much of the volume in a barred galaxy the stars are in orbits that oscillate about a single family of closed orbits. However, near resonances there are not only many families of closed orbits but also regions where there are no closed orbits. The area of a bar which is not covered by the major families of closed orbits is generally small (e.g., Athanassoula 1992), and so the effects of the resonances are limited. The complicated behavior of orbits near resonances increases the stellar velocity dispersion, so the stellar population will appear to be well mixed. This results in a smoothing of the color variations across the resonances. Examples of this can be seen in Buta (1990), where color maps show a smooth transition between orbits aligned perpendicular and parallel to the bar. Over much of

a bar the approximation that all orbits are near closed orbits should be valid, and so it is possible to use the difference between isophote and orbit shapes to derive dynamical information. Where this approximation fails, a smooth variation in ellipticity should be observed in the galaxy, and equation (8) will give a spurious low value for Φ_1.

In this section we have explored the limit of small ellipticity. However, even when the orbits are not elliptical, the speed variation along the orbit can still be determined from variation in density and the area element in a segment along the orbits. The orientation of velocity vectors can be found from the shapes of the orbits, and the speed is determined from the isophotes. If the rotation curve is known, the entire galaxy potential can in principle be completely reconstructed.

2.2. *A Model Galaxy Example*

In this subsection we demonstrate with a model galaxy that when the orbits are noncircular the isophotes and isochromes have different shapes.

Using Newton's equations, we have integrated stellar orbits in a logarithmic potential of the form $\Phi = v_c^2 \ln s$, where $s = [x^2 + y^2(1-\epsilon)^2]^{1/2}$ and ϵ sets the size of the nonaxisymmetric perturbation. For $\epsilon = 0$ this potential gives a flat rotation curve with circular velocity v_c. Over a range of radius, closed orbits were found by minimizing the difference in positions along the major axis before and after one revolution about the nucleus. A density array was constructed from the positions of the stars at equal time steps along each orbit by assuming that the density along the major axis a of each orbit was exponential, $\Sigma(a) \propto \exp[-a/h(\lambda)]$, with scale length $h(\lambda)$ a function of wavelength λ.

In Figure 1 a model is displayed with color maps. Figure 1*a* shows isophotes for a model with identical orbits but with different scale lengths. Note that the shape of the isophotes depends on the scale length. Figure 1*b* shows isophotes and color contours. The color contours are coincident with the closed orbits, and have a different ellipticity than the isophotes.

2.3. *Underlying Assumptions and Caveats*

We have assumed that the stellar population in the galaxy is an evenly distributed, dynamically relaxed, and mixed stellar population. One important effect not considered here is the role of star formation. If stars are formed quickly compared to the orbital timescale, then the colors observed will trace the local occurrence of star formation and not directly provide information about the stellar dynamics. This problem could be made less severe by studying near-infrared images which are less sensitive to the presence of young stars and instead trace a more evenly distributed older stellar population.

The stellar velocity dispersion (both in the plane and vertical), if it is not small compared to the rotational velocity, will also affect both the projected surface density and isochromes. The phenomenon discussed here cannot be used to detect noncircular motion near a galaxy bulge or in a very early type galaxy because these systems are not planar and have a large velocity dispersion compared to their rotational velocity.

The orbits of gas and dust when there are no strong shocks present should be almost identical to the closed stellar orbits, so isochromes should still trace the shapes of the closed orbits even when a moderate amount of dust is present. However, when shocks are present in the interstellar medium of a galaxy such as is found in dust lanes in barred galaxies, it would be extremely difficult to detect subtle effects due to population gradients if the color maps were dominated by extinction. Strong spiral structure will also cause difficulties for a number of reasons. Isophote ellipticities and position angles are affected by the spiral arms, which can have a lot of extinction and many young stars.

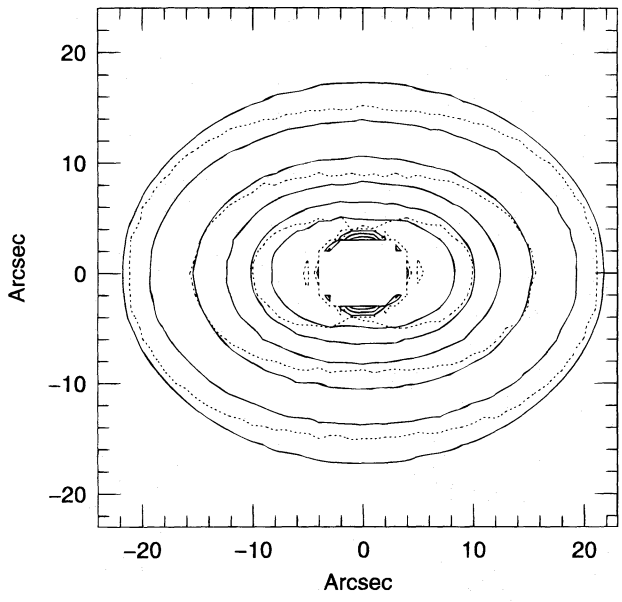

FIG. 1*a*

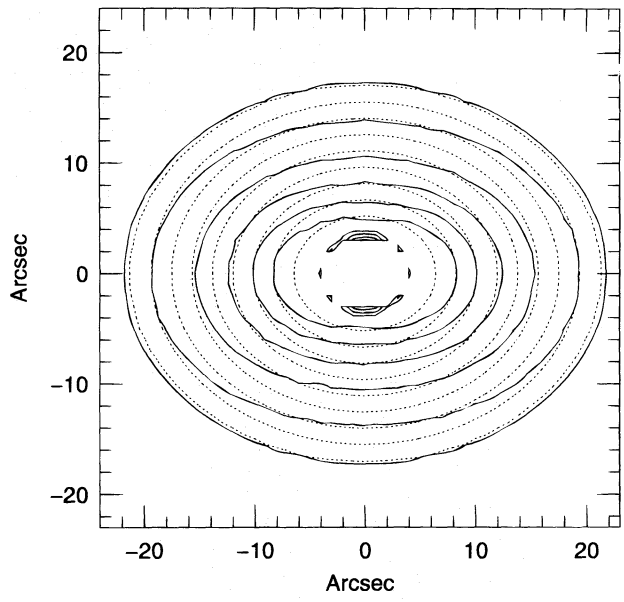

FIG. 1*b*

FIG. 1.—(*a*) Isophotes for the model galaxy described in § 2.1. Shown are isophotes for exponential disk scale lengths $h = 1$ (*solid lines*) and $h = 2$ (*dotted lines*). For this model $\epsilon = 0.2$ and $v_c = 1$. Note that the isophote shapes depend on the exponential disk scale length. (*b*) Isophotes (*solid lines*) and isochromes (*dotted lines*) for the model galaxy. Isophotes are shown for exponential scale length $h = 1$. Note that the isophotes differ from the isochromes.

TABLE 1

SUMMARY OF OBSERVATIONS

Date	Galaxy	Photometric?[a]	J^b	H^b	K^b	B^b	V^b	R^b
1992 Nov 2.....	NGC 1800	Yes	20	...	18	...	...	...
1992 Nov 3.....	NGC 1800	Yes	...	20	24	...	...	...
1994 Nov 1.....	NGC 1800	Yes	...	...	...	15	11	6
1992 Nov 5.....	NGC 7764	No	20	20	48	...	...	...
1993 Oct 4	NGC 7764	Yes	5	2	2	...	...	...
1994 Nov 1.....	NGC 7764	Yes	...	...	...	12	6	6

[a] "Yes" means the night was photometric.
[b] On-source exposure times given in minutes.

We note that in the presence of noncircular orbits an inclined galaxy will have twists in both the isophotes (e.g., de Zeeuw & Franx 1989) and the isochromes. Warped galaxies also have twists in the isophotes; however, if the orbits are close to circular, then the isophotes should have the same ellipticity as the isochromes even if the isophotes are twisted. At high inclination the thickness of the stellar disk will also affect the ellipticities of the isophotes, so this effect can only be used for galaxies at low inclination.

3. OBSERVATIONS

Two dwarf galaxies NGC 1800 and NGC 7764 were observed in the near-infrared J, H, and K bands and in the visible B, V, and R bands.

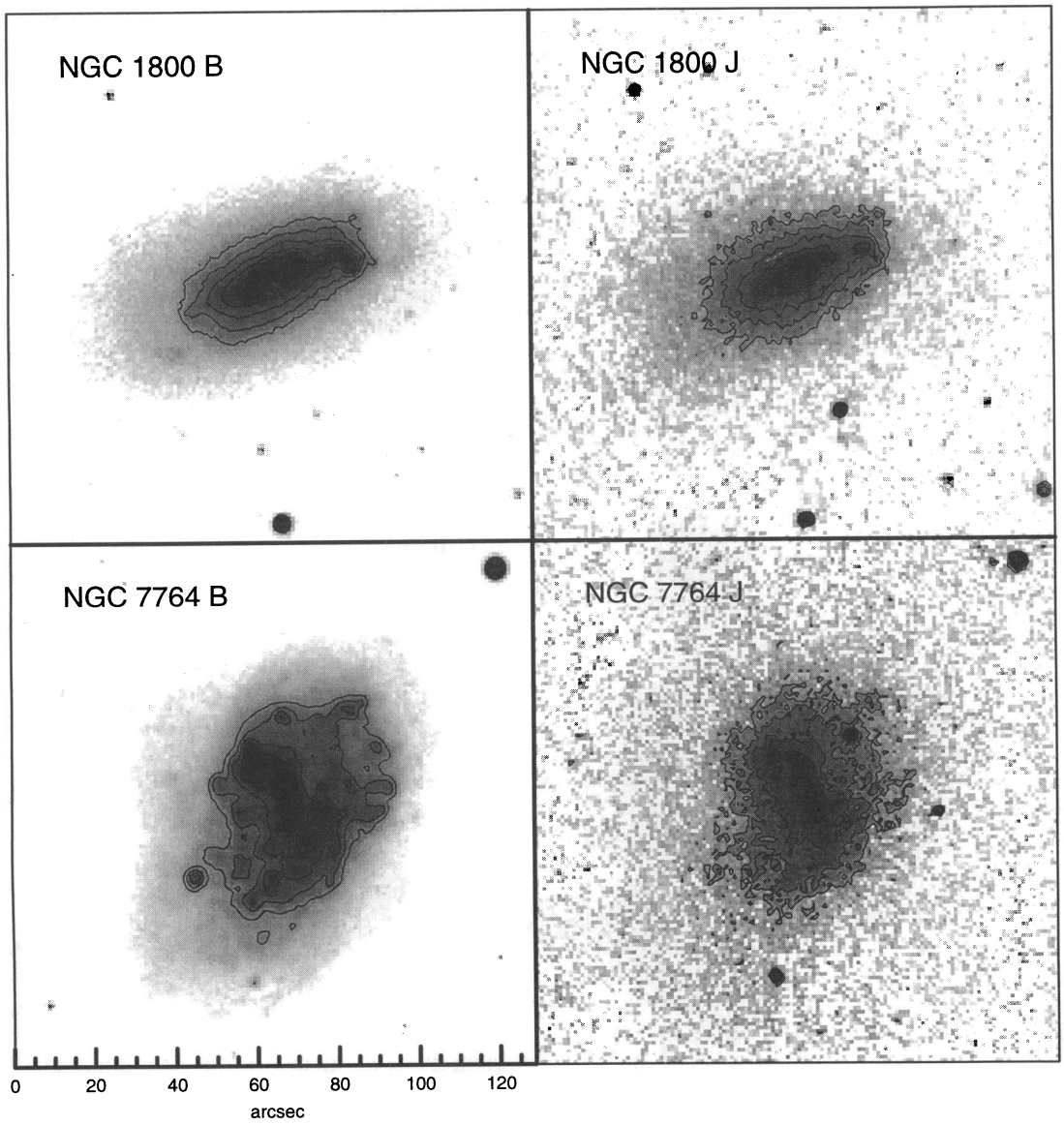

FIG. 2.—Gray-scale images of the two dwarf galaxies NGC 1800 and NGC 7764 in the B and J bands. Contours are 0.5 mag apart with brightest contours at 15.5 mag in the J band and 13.2 mag in the B band.

3.1. *Near-Infrared Images*

The J, H, and K images were obtained on the 1.0 m Swope Telescope at Las Campanas Observatory with the NICMOS3 infrared array (Persson et al. 1992), which covered a field of $3'.9 \times 3'.9$, with a spatial scale of $0''.92$ pixel^{-1}. Individual images were taken with an exposure time of 60 s in J, 20 or 30 s in H, and 15 s in K. The observations are summarized in Table 1. For these observations, sky was observed for a total integration of about half of the total on-source integration time. Flat fields were constructed from median filtered sky frames. Images were aligned to the nearest pixel and combined after a slight nonlinearity correction, flat fielding, and sky subtraction.

The images were calibrated on the CTIO/CIT system using standard stars from Elias et al. (1982). For NGC 7764 we calibrated the long-exposure images observed under nonphotometric conditions by comparing the magnitudes of five field stars in the long-exposure images with the magnitudes measured on short-exposure images observed under photometric conditions. From the scatter in the magnitudes of these stars and the standards, we estimate our accuracy of the calibration to be within ± 0.05 mag. There is good agreement between our calibrated images of NGC 1800 and published aperture photometry by Hunter & Gallagher (1985) with an aperture diameter of $23''$. We find that our J, H, and K magnitudes are brighter than those of Hunter & Gallagher (1985) by 0.07, 0.08, and 0.02 mag at J, H, and K, respectively. The FWHMs of stars in the final images are $\sim 2''.5$, which is larger than that caused by seeing because of the shifting of individual images required to construct the final images.

3.2. *Optical Images*

The B, V, and R images were observed under photometric conditions on the 0.9 m telescope at CTIO, using a 1024×1024 pixel CCD with a spatial scale of $0''.40$ pixel^{-1}. Individual images were taken with an exposure time of 300 s in B, 200 s in V, and 120 s in R. A linear overscan bias and dark images were subtracted from the individual images, which were then flat-fielded using flat fields constructed from means of dome flats. Cosmic-ray events were removed using interactive median filtering. The final images were made from averages of the individual images. The calibration was done using standard stars from Landolt (1992). We estimate our accuracy to be $\sim \pm 0.04$ mag. There is good agreement between our calibrated images of NGC 1800 and published aperture photometry by Gallagher & Hunter (1987) with aperture diameters of $57''$ and $130''$. We find that our B, V, and R magnitudes are brighter than those of the above authors by 0.03, 0.03, and 0.02 mag at B, V, and R, respectively, but consistent within the errors.

3.3. *Registered Images and Color Maps*

To transform the optical and infrared images to the same pixel scale, orientation, and resolution, we used linear transformations which included a rotation and a scaling term as well as a shift. These transformations were derived from measurements of centroids of stars in the field. We estimate that our registration is good to within $0''.3$ across the images based upon the standard deviation of centroids of the field stars of the registered images. The images were then smoothed so that stars had the same FWHM in all bands. Registered, resampled, and smoothed optical and near-infrared images are displayed in Figure 2.

4. APPLICATION TO NGC 1800 AND NGC 7764

Both NGC 1800 and NGC 7764 have blue central regions and a patchy amorphous appearance, probably because of recent star formation. Except for two bright spots in the images of NGC 1800, the isophotes are regular and elliptical even in the B band. The H I velocity field of NGC 1800 suggests that this galaxy harbors a bar (Hunter, van Woerden, & Gallagher 1994). NGC 1800 has a disturbed Hα morphology with plumelike and looplike features (Hunter et al. 1994). However, the morphology of the visible images does not resemble the morphology of the Hα emission so that even in the visible images primarily what is seen is a smooth underlying, evenly distributed stellar population. The appearance of the optical images is almost identical to that of the infrared images. This is consistent with the interpretation that primarily what is seen in all bands is an evenly distributed, dynamically relaxed stellar population. This assumption is required to interpret a difference in the ellipticities of the isophotes and isochromes as being due to noncircular motion and not due to local star formation.

In Figure 3 we show $B-V$ color contours plotted with the R band isophotes for NGC 1800 and NGC 7764. Optical bands were chosen for measurement of ellipticities because of their higher signal-to-noise ratio. In both galaxies there is a smooth difference in morphology between the color maps and the isophotes. We checked that this difference is not a result of improper sky subtraction by considering all sky values for both colors that are within our estimated errors for the sky value.

NGC 1800 has color contours that are more elliptical than the isophotes. If the stars were on circular orbits in this galaxy, the color isophotes would lie on top of the isophotes, so the difference in the two contour maps is good evidence that NGC 1800 does harbor a bar, and we confirm the suggestion of Hunter et al. (1994) that NGC 1800 has a bar. We expect that in each closed stellar orbit the density should be largest along the bar where the velocity is lowest. However, if the radial gradient of the density is large and the ellipticities of the orbits vary, then the isophotes may be less elliptical than the isochromes (see eq. [2]).

In Figure 4 we plot ellipticities and position angles as a function of radius for both galaxies for the optical bands where a higher signal-to-noise ratio permitted isophote fitting. In NGC 1800 we note that the ellipticities of the isophotes in the different filters are equal at $\sim 50''$. This would be consistent with the galaxy having bar corotation radius at this radius. This radius is also suggested as the approximate location of corotation from the H I velocity field because the isovelocity contours only twist inside this radius.

Using equations (3.12)–(3.14) in de Zeeuw & Franx (1989), which describe the projected ellipticity and position angle of an ellipse given its orientation and true ellipticity and position angle, we find that an inclination $\sim 81°$ (close to edge on) and position angle $\phi \sim 70°$ come closest to predicting the range of ellipticities and position angles observed as a function of radius in the B band. In the principal plane of the galaxy this position angle, ϕ, is defined to be the angle between the line of sight (projected onto this plane) and the major axis of the gravitational potential (as in de Zeeuw & Franx 1989). The inclination is set by the point where the ellipticities cross at $50''$, and the position

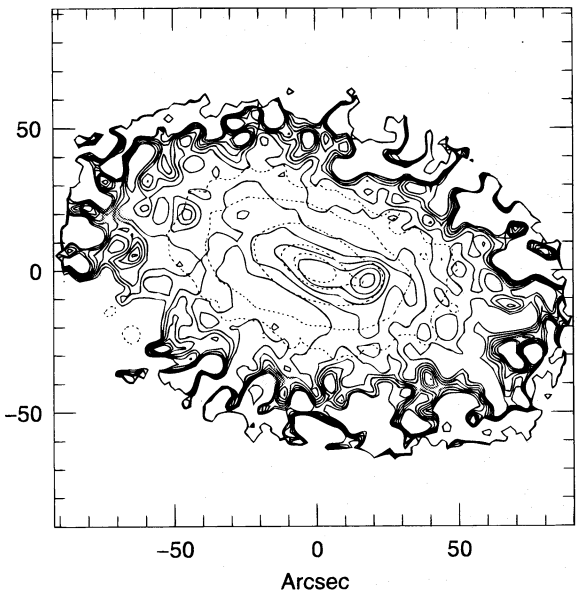

FIG. 3a

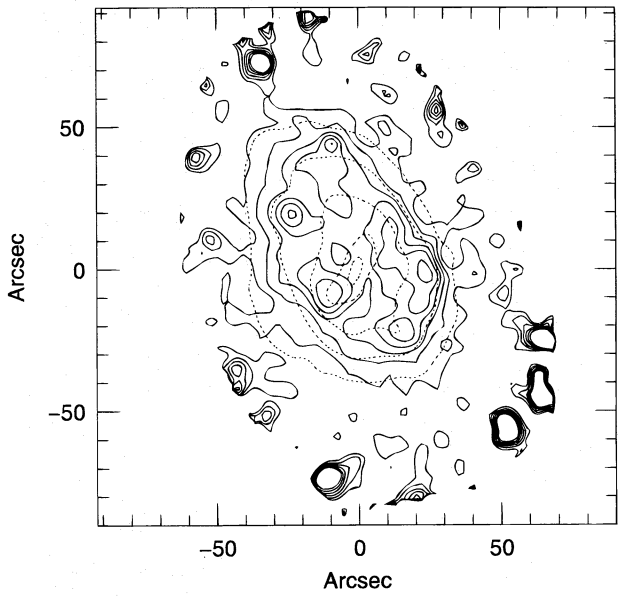

FIG. 3b

FIG. 3.—(*a*) Contour plots show the *R*-band isophotes (*dotted contours*) and $B-V$ color maps (*solid contours*) for NGC 1800. Note that the isochromes do not lie on top of the isophotes. (*b*) Same as (*a*), but for NGC 7764.

angle was chosen so that the position angle and ellipticity observed at every radius were consistent with an ellipse viewed at these projection angles. Using these projection angles, we estimate true ellipticities for the orbit $\epsilon_r \sim 0.35$ at 30″ and ~ -0.1 at 60″, and for the isophotes at the *B* band $\epsilon_D \sim 0.2$ at 30″ and ~ -0.15 at 60″. For an exponential scale length at the *B* band of $r_D \sim 10''$, which we have measured from the major axis of the *B*-band image, using equation (3) we estimate that Φ_1 ranges from $0.45v_c^2(1-\Omega_p/\Omega)$ at 30″ to $0.3v_c^2(1-\Omega_p/\Omega)$ at 60″. That the bar potential varies smoothly but is more elliptical within the bar than outside it is consistent with estimates of the

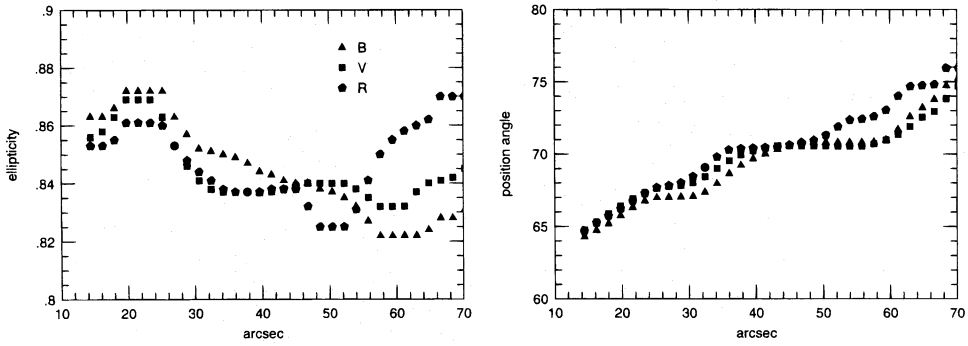

FIG. 4a

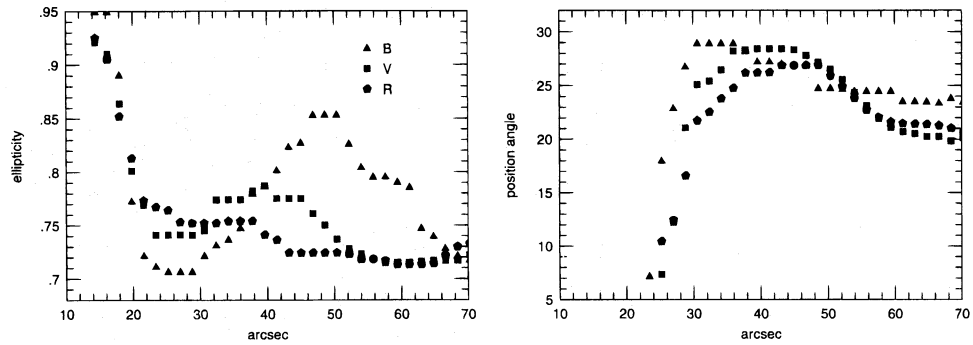

FIG. 4b

FIG. 4.—(*a*) Plotted are the ellipticities of the isophotes and their position angles (from north) as a function of radius for NGC 1800. (*b*) Same as (*a*), but for NGC 7764. Note that the ellipticities cross at around 50″ for NGC 1800 and at around 46″ for NGC 7764. This is consistent with bars ending at these radii. Contour fitting was done with the software VISTA on images with stars removed.

gravitational potential in barred galaxies (e.g., Quillen, Frogel, & González 1994). These estimates are meant to be primarily illustrative, since they are crude. A better data set on a galaxy that is closer to face-on would warrant a more detailed study.

In NGC 7764's color map we can see a blue star-forming ring that is outside the end of the bar. The spotty appearance implies that we are seeing local star formation in the ring, so that the light may not trace a conserved quantity in an orbit, although we do expect that the stars have formed along closed orbits. No difference between the isochromes and the isophotes were found within the bar because there is little color gradient in this region (see Fig. 3). We can, however, use the ellipticities of the isophotes to find the end of the bar. The ellipticities are about the same at a radius of $\sim 40''$. This is consistent with this ring being at the corotation radius (see Fig. 4).

5. SUMMARY AND DISCUSSION

In this paper we have introduced a way to use color gradients to detect the presence of nonaxisymmetric dynamical motion such as a bar or a triaxial halo. In a galaxy with both a color gradient and noncircular motion, the shapes of closed orbits should follow the isochromes, and the ellipticity of the isophotes should vary as a function of wavelength. The difference between isophote and orbit ellipticity should be largest where the surface brightness gradient is shallowest. From the position angles and ellipticities of the isophotes at different radii the orientation of the galaxy can be determined. Once the orientation of the galaxy is known, the strength of the nonaxisymmetric component of the gravitational potential can be directly measured.

To illustrate this phenomenon we have constructed a simple model with a flat rotation curve. This model shows that when the orbits are elliptical, the isophote shapes depend on the exponential scale length of the disk and that the isophotes are not coincident with the isochromes.

We search for this phenomenon in two dwarf galaxies. In NGC 1800 the isochromes have a different ellipticity than the isophotes, implying that there is a bar in this galaxy which has previously only been suggested from the H I velocity field. The ellipticities of the isophotes in different bands are equal at a radius of $50''$, which suggests that the bar ends at this radius. Using the observed ellipticities and position angles at different radii, we have estimated the orientation of the galaxy. From the true ellipticities we find that the strength of the nonaxisymmetric component of the potential near the end of the bar decreases as a function of radius, as expected in a barred galaxy.

In NGC 7764 there is little color gradient along its bar, so we do not detect the presence of noncircular motion within the bar. At the end of the bar there is a blue ring undergoing star formation where the ellipticities of the isophotes in different bands are equal. This is consistent with this ring being near the corotation radius.

The recent availability of deep multiband images of galaxies suggests a number of settings for an investigation of the phenomenon introduced in this paper. Since exponential disk radii differ as a function of wavelength by a few percent (de Jong 1994), it should be possible to detect noncircular motion in the outer parts of disk galaxies where dark matter is dominant. The largest color gradient can be achieved by comparing optical and infrared images; however, using only infrared images may be desirable because the images should be less affected by recent star formation. Rix & Zaritsky (1995) have recently discovered that most galaxies are lopsided. We suggest that color gradients can be used to constrain the lifetime of such asymmetries. Comparing color contours to the shape of closed orbits integrated in the gravitational potential of a barred galaxy (e.g., as in Quillen et al. 1994) could constrain formation mechanisms for the bar.

In elliptical galaxies isophote ellipticity and orientation angle have been observed to depend upon wavelength (e.g., Peletier 1989). By summing over a library of orbits, the shapes of elliptical galaxies could also be measured from color maps.

Since many rings of ring galaxies are located where the dark matter contribution is significant, this technique can be used to compare the morphology of dark matter with that of non–dark matter. In the ring of a ring galaxy which has an inner bar, the gravitational potential is not circular because of the bar. Since these galaxies typically have color gradients, the effect described in this paper should be detectable in such a situation. The ellipticity of the potential can be measured as a function of radius and directly compared to the ellipticity of the potential predicted from the light distribution.

We are grateful to Roberto Aviles for obtaining the *B*, *V*, and *R* images for us. We acknowledge helpful discussions and correspondence with G. Rivlis, R. Q. Rivlis, R. J. Buta, B. Elmegreen, H.-W. Rix, A. Gould, and D. Zaritsky. The OSU galaxy survey is being supported in part by NSF grant AST 92-17716. The Las Campanas Observatory infrared camera was built with partial funding from NSF grant AST 90-08937 to S. E. Persson. J. A. F.'s research is supported in part by NSF grant AST 92-18281. A. C. Q. acknowledges the support of a Columbus fellowship. J. A. F. thanks the Physics Department of the University of Durham and PPARC for support via a Senior Visiting Research Fellowship. We thank the referee, J. S. Gallagher, and Linda Sparke for helpful comments and suggestions which improved the paper.

REFERENCES

Athanassoula, E. 1992, MNRAS, 259, 328
Binney, J., & Tremaine, S. 1987, Galactic Dynamics (Princeton: Princeton University Press)
Buta, R. J. 1990, ApJ, 351, 62
de Jong, R. S. 1994, Ph.D. thesis, Rijksuniv. Groningen
de Zeeuw, P.T., & Franx, M. 1989, ApJ, 343, 617
Elias, J. H., Frogel, J. A., Matthews, K., & Neugebauer, G. 1982, AJ, 87, 1029
Franx, M., & de Zeeuw, P. T. 1992, ApJ, 392, L47
Franx, M., van Gorkom, J. H., & de Zeeuw, P. T. 1994, ApJ, 436, 642
Gallagher, J. S., III, & Hunter, D. A. 1987, AJ, 94, 43
Hunter, D. A., & Gallagher, J. S., III. 1985, AJ, 90, 1457
Hunter, D. A., van Woerden, H., & Gallagher, J. S., III. 1994, ApJ, 91, 79
Landolt, A. U. 1992, AJ, 104, 340
Peletier, R. 1989, Ph.D. thesis, Rijkuniv. Groningen
Persson, S. E., West, W. C., Carr, D., Sivaramakrishnan, A., & Murphy, D. 1992, PASP, 104, 204
Quillen, A. C., Frogel, J. A., & González, R. A. 1994, ApJ, 437, 162
Quillen, A. C., Ramírez, S. V., & Frogel, J. A. 1995, AJ, 110, 205
Rix, H., & Zaritsky, D. 1995, ApJ, 447, 82
Sackett, P. D., Rix, H., Jarvis, B. J., & Freeman, K. C. 1994, ApJ, 436, 629
Staveley-Smith, L., Bland, J., Axon, D. J., & Davies, R. D. 1990, ApJ, 364, 23
Thomsen, B., & Baum, W. A. 1989, ApJ, 347, 214